Volume 2, Number 1, 2009. pp. 59-72

Jordan Journal of Physics

ARTICLE

Obstacle Exclusion from X-Ray CT Angiography Data for 3D Image Diagnosis

A. M. Alyassin

Department of Physics, Yarmouk University, Irbid, Jordan.

Received on: 13/12/2008; Accepted on: 1/3/2009

Abstract: A fast and novel technique was developed to exclude obstacle data from a single Computed Tomography Angiography (CTA) data set. The data was minimally processed to preserve the majority of the CTA data in its original form, especially the vascular information. The technique was based on a newly developed adaptive composite mask which used multi-step image processing techniques. Excluding a structure like-bone from CTA data can improve several three dimensional (3-D) visualization techniques such as volume rendering, shaded surface display, or maximum intensity projection to better render the vascular data unveiling any aneurysms or calcifications in a clear manner. This enhancement in angiogram visualization is expected to increase the sensitivity of clinical diagnoses. The proposed technique demonstrated obstacle free 3-D vessel visualization in ten different CTA data sets.

Keywords: CT angiography, Obstacle data exclusion, Segmentation, Visualization, Bone removal.

Introduction

Conventional X-ray angiography is the gold standard in terms of diagnostic accuracy, but it has risks associated with it [1, 2]. Therefore, non-invasive or minimally invasive techniques including computed tomography (CT) are of interest to radiologists evaluating the vascular system. In CT, multiple contiguous or partially overlapping sections of tissue are reconstructed. CT is known to provide tomographic high contrast between bony structures (i.e. skull) and soft tissue (i.e. brain). This high contrast is useful in many medical applications. However, visualization of blood vessels using conventional CT is currently a very difficult task due to the fact that CT Hounsfield numbers of vessels and their surrounding soft tissues (i.e. brain tissues of white and grey matters) are similar. In CTA however, the contrast of the vessels compared to the surrounding tissue is enhanced. This enhancement is due to the use of a contrast agent injected before the CT scan. Consequently this increases the vessels' X-ray attenuation coefficients leading to an increase in the vessels' CT number (CTN), thus enhancing the contrast with surrounding tissues [3]. Clinicians are then able to visualize vessels in 2-D tomographic views. Vessels, however, are 3-D tree-like structures, their visualization in 2-D is still a very tedious task.

3-D visualization techniques, like maximum intensity projection (MIP), surface shaded display (SSD), or volume rendering (VR) are known techniques in visualizing 3-D data [4,5,6,7,8]. However, the high CT numbers (CTNs) for bone create a major barrier in visualizing blood vessels. In addition, excluding these high CTNs cause difficulty in retaining vessel filled with contrast agent. This is due to the overlapping CTN distributions for bone and contrast filled vessels. This overlap in the CTN distributions

Corresponding Author: A. M. Alyassin. **Email**: alyassin@yu.edu.jo.

is mainly due to the following two conditions. First, part of the vessel CTN distribution falls in the bone CTN distribution. Some of this can be attributed to the vessel's calcification and should not be ignored. Second, part of the bone CTN distribution also falls into the vessels CTN distribution. Most of this is due to partial volume averaging, where the boney volumes do not end abruptly but rather fall in a gradual fashion to the background region or surrounding tissues.

Current techniques in CTA employ semi-automatic editing techniques to eliminate bones [9]. The tracing is usually performed in two different modes [10]. In exclusive editing mode, experts trace regions selected for removal where as in the inclusive mode, they trace regions selected for inclusion. These approaches may introduce distortion of information when the connectivity algorithm uses a threshold which is too low to exclude bones physically touching the vessels [11]. Such editing also requires a lot of operator time (15 – 30 minutes). In most cases, the results are influenced by experience and personal bias of individual operators. Furthermore, the method was not good at depicting aneurysm.

In an effort to reduce the operator time, investigators have developed hybrid semi automated editing programs [12]. In these techniques, an automated 2-D segmentation procedure is performed to produce a set of labeled images. Each segment becomes associated with a distinct label. The then user views a small number of labeled images and selects segments of interest by pointing and clicking with a mouse. This activity triggers a connectivity algorithm that collects related segments for inclusion in the edited sections. Selected segments are then used as a mask to exclude the corresponding voxel values from the raw images. This method is computationally very intensive and currently not suited for clinical practice.

Another approach proposed in literature involves the use of warped matching for digital subtraction of data sets corresponding to pre- and post-contrast injection [13]. The authors have developed a 3-D flexible registration procedure which was inspired by a 2D technique introduced by Van Tran and Sklansky [14, 15]. This method not only requires the availability of two data sets which increases the radiation dose to the patient, but it is computationally too involved to be of use in routine clinical practice.

Currently there is a need for a fast segmentation technique which would totally remove bone from a single CTA data set while preserving vessel information in its original form without adding any spurious image processing artifacts. The technique described here will show the feasibility of such a technique. It involves steps necessary for bone segmentation and the steps needed to speed up the computations using appropriate approximations. This paper is a continuation to an initial work that was presented at an SPIE conference [16].

Methods

The proposed method consists of a few steps which lead to total exclusion of connected bone from a single CTA data set while preserving vessel data information. Fig.s 1 and 2 show flow charts of the algorithm's main preparation steps and the image processing steps used in the developed technique, respectively.

Image Data Acquisition

Seven subjects were imaged once in the head and three subjects were scanned once in the abdomen using the G.E. Helical HiSpeed CT Scanner. The CT scanner was set to 140 KVp and the mAs settings ranged from 180 to 200 between subjects. The data was acquired post to a specified time delay from the time of the contrast agent injection. The time delay between imaging and injection was approximately 15 seconds. Isovue contrast agent was used. Its amount ranged between subjects from 300 to 370 cc.

The acquired head data sets consisted of a series of CTA images covering the imaged volume which included the Circle of Willis region, and the abdomen data sets covered the kidneys and lungs. Slice thickness was 1 mm with 0.5 mm overlap. Between the subjects, the field of view ranged from 160 to 220 mm, the matrix size along x, y, and z was 512x512xN where N ranged from 60 to 119 slices, and the voxel aspect ratio ranged from 4:4:1 to 2:2:1.

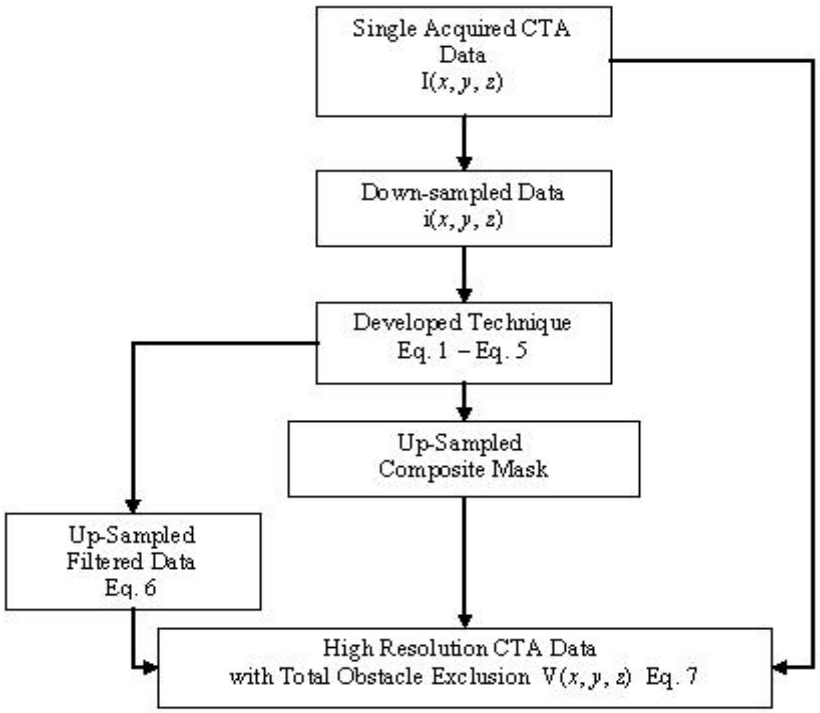

FIG. 1. Flowchart illustrating the preparation steps for the developed technique. The equation number shown in each box refers to the equation used in processing the data.

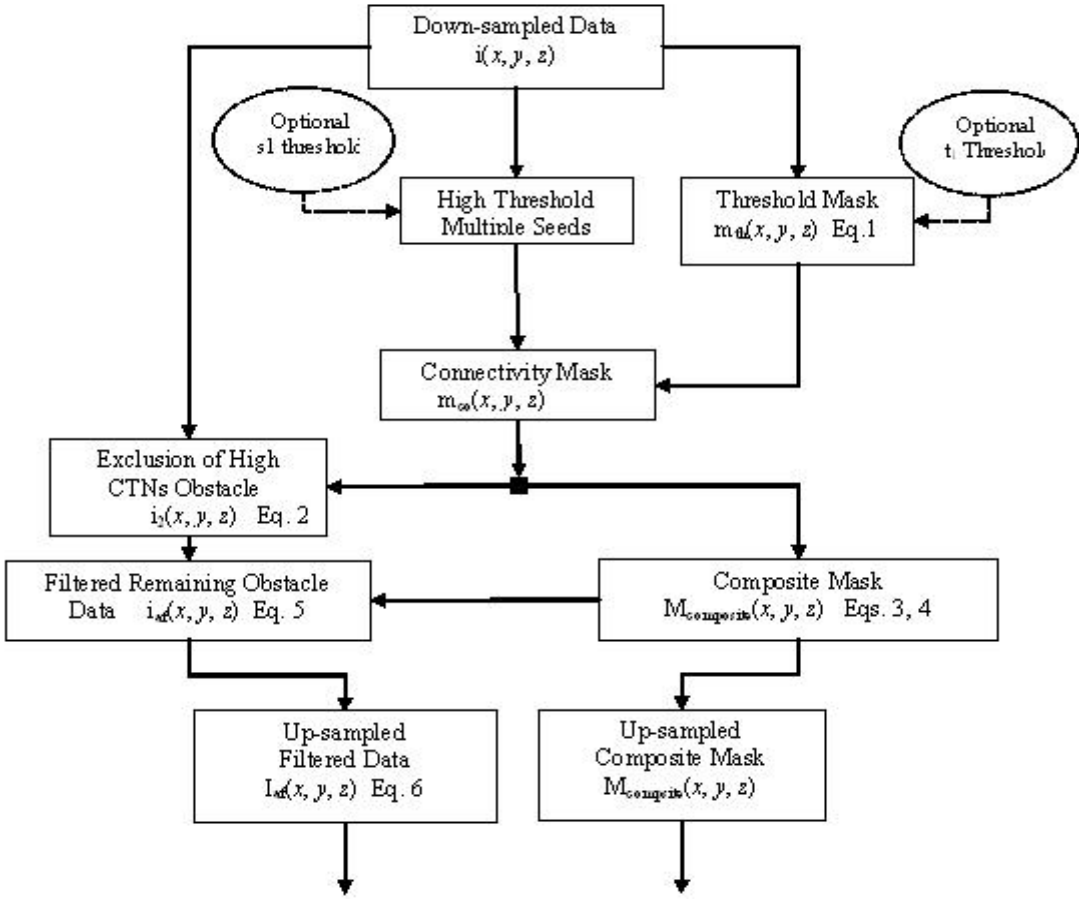

FIG. 2. Flowchart illustrating the connectivity of the main steps for the developed technique. The equation number shown in each box refers to the equation used in processing the data. The outputs of the dotted line box will feed as two of the three inputs shown in the final stage of Fig. 1. Note also the optional t1 and s1 thresholds for optimal results.

In this paper, I(x, y, z) will be used to represent the original input data of the imaged volume and V(x, y, z) will be used to represent the final output CTA data. The (x, y, z) point represents a voxel location in the 3-D data volume and I and V represent the CTN at (x, y, z) location.

Data Down-Sampling

I(x, y, z) data was down-sampled to a lower spatial resolution along x, y, and z. The lower resolution data is referred to here with a lower case i(x, y, z). I(x, y, z) data was down-sampled to an isotropic i(x, y, z) data where the i(x, y, z) voxel aspect ratio (VAR) was 1:1:1. For instance, if VAR was 4:4:1 in I(x, y, z), then a 4x4x1 kernel was used in the down-sampling process. Note that the output of this kernel was reduced to one voxel in i(x, y, z) with a value equal to the maximum CTN of the voxels in the kernel.

Threshold Mask

To estimate a threshold for bone removal, it was necessary to know the CTN distribution of other visible tissues in a CTA data. The main tissues that could be visualized in a CTA data of the head were the skull, the brain, vessels, calcifications, and air cavities or air surrounding the head. The average CTN for these tissues were 1748, 61, 273, 826, and -954 respectively. These numbers were calculated from the acquired CTA data sets. For each specific tissue, a region of interest (ROI) was drawn in an area internal to the tissue. The average CTN value of the ROI was then calculated. This calculation was repeated on five different CTA data sets, and the mean value for these calculations was used to indicate the tissue's CTN. A similar technique was done for the abdomen data sets. The main visualized tissues in the abdomen were cortical bone, spongy bone, liver, kidney, vessels, and air. The average CTNs for these tissues were 657, 120, 107, 333, 483 and -954 respectively. Note that the skull cortical bone CTN was higher than the abdomen cortical bone CTN. This is due to the higher density of the cortical bone in the skull. Fig. 3 shows CTA images of head and abdomen and corresponding line profiles drawn on the images.

A threshold mask $m_{th}(x, y, z)$ was generated using Eq. 1 on the down-sampled data i(x, y, z) with a default $t_1 = 400$. For optimal results, however, the threshold value t_1 ranged from 350- to 500 CTNs and can be set and adjusted by the user. The voxels that are set in this mask corresponded to voxels containing mainly cortical bone in i(x, y, z).

$$(x, y, z) \in r$$

where (x, y, z) is a location in the subsampled data spacer.

$$m_{th}(x, y, z) = \begin{cases} 1 & \text{if} \quad i(x, y, z) > t_1 \\ 0 & \text{otherwise} \end{cases} \qquad (1)$$

Eq. 1 marks every voxel having a CTN higher than t_1. Although t_1 was high enough to mark voxels containing mainly cortical bone, some voxels containing calcifications in the i(x, y, z) have CTNs high enough to also be set in the m_{th} mask.

Connectivity Mask

A $m_{co}(x, y, z)$ mask was generated by applying a 26-neighbor connectivity technique on the m_{th} mask [17]. This step un-marks voxels that corresponded to non bony tissue (i.e. calcifications) and retains marked voxels corresponding to connected cortical bone in the m_{th} mask as shown in the following pseudo-code.

set the mutiple seeds into $m_{co}(x, y, z)$ mask $= 1$;

growseeds $= 1$;

while { *growseeds* }

{

growseeds $= 0$;

// have to grow at least one seed when marching through the data

$$\sum_{z=2}^{n-1}\sum_{y=2}^{n-1}\sum_{x=2}^{n-1}\left[\begin{array}{l}\text{if } m_{th}(x,y,z)=1 \text{ and } m_{co}(x,y,z)=1;\\ \text{then } \sum_{k=-1}^{1}\sum_{j=-1}^{1}\sum_{i=-1}^{1} m_{co}(x+i, y+j, z+k)=1;\\ \text{and } growseeds=1;\end{array}\right]$$

// where n is the dimention of the down - sampled data, note that the $\sum$ *sign*

// starts from 2 to n - 1 to account for boundary limits in the data

}

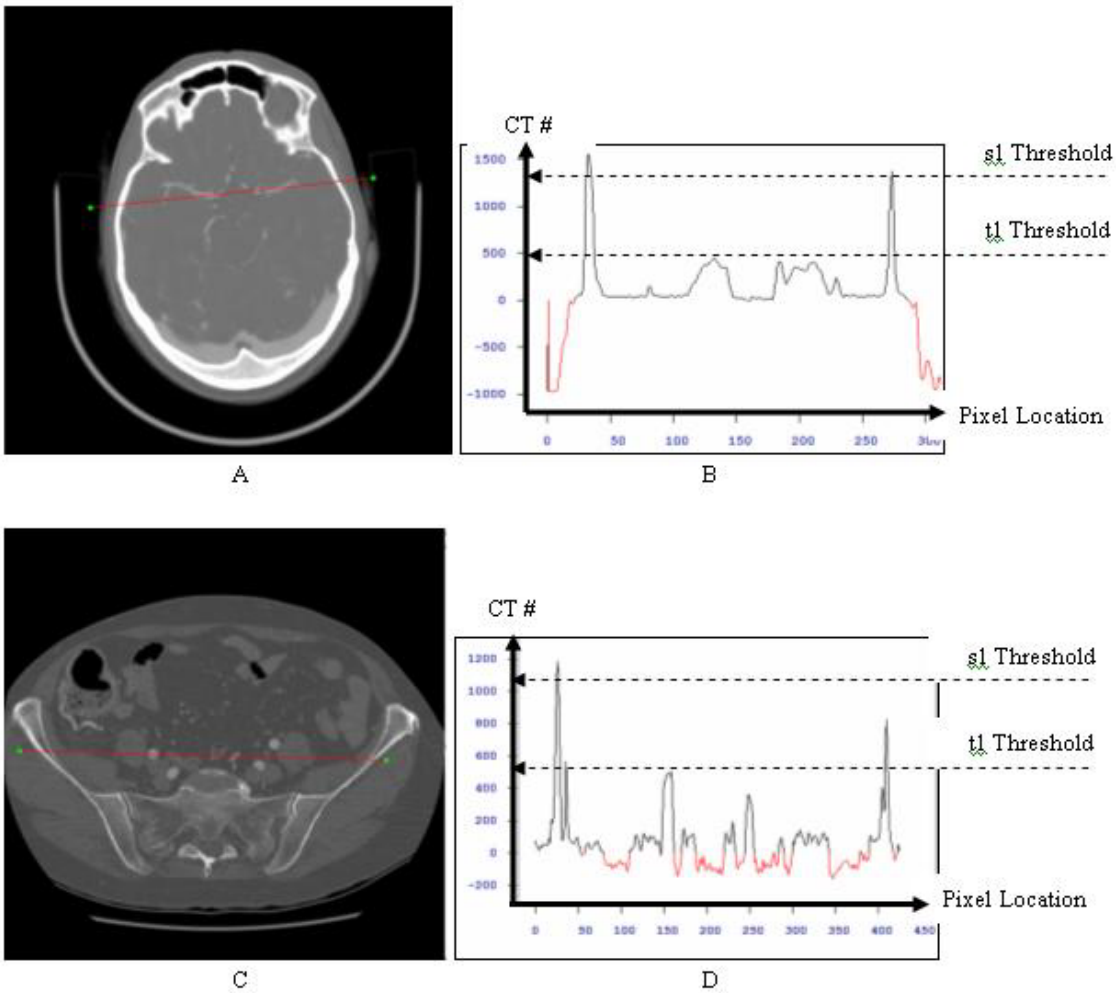

FIG. 3. Illustrates CTA images for the head and abdomen. Fig.s 3A and 3B show a CTA head image and the corresponding line profile respectively. Fig.s 3C and 3D show a CTA abdominal image and the corresponding line profile respectively. Note the t1 and s1 thresholds used in the technique.

Note that the connectivity technique requires seeds to grow the connected regions. Therefore, multiple seeds were used for this step. The coordinates (x, y, z) for these multiple seeds were identified using a threshold technique with a default (s_1) value. The default threshold (s_1) was equal to 90% of the maximum CTN in each data set but it may also be set and adjusted by the user. Fig. 3 shows the relative t_1 and s_1 CTN values in line profiles. Any voxel having a CTN higher than s_1 was used as a seed in the connectivity technique to grow the high CTN bone region.

Exclusion of High CTN Obstacle Data

CTA data $i_2(x, y, z)$ was generated using $i(x, y, z)$ and m_{co} mask as shown in Eq. 2,

$$i_2(x,y,z)=\begin{cases} i(x,y,z) & \text{if } m_{co}(x,y,z)=0 \\ t_0 & \text{if } m_{co}(x,y,z)=1 \end{cases} \quad (2)$$

where t_o is the vessel surrounding tissue mean CTN as can be deduced from Fig. 3. In our case the t_0 value had a CTN of 50.

Transition Region and Composite Mask

A transition region was generated by dilating the connectivity m_{co} mask with B_{3x3x3} kernel using its 26-neighbors [18], as shown in Eq. 3:

$$\left.\begin{aligned} & m_{composite}(x,y,z)=m_{co}(x,y,z)\oplus B_k \\ & \begin{cases} \text{where} \quad k=3\times 3\times 3 \\ \textit{and} \ \oplus \text{ is the dilation operator} \end{cases} \end{aligned}\right\} \quad (3)$$

Where B represents the kernel and k represents its size. Fig. 4 illustrates a mockup 2-D simulated image for the formation of a composite mask. Although, there are different techniques to perform dilation [19], the approach used to accomplish this dilation task is based on the center voxel value of the kernel B_{3x3x3}. The kernel marches and shifts through the entire m_{co} mask data. If the center voxel of the kernel B_{3x3x3} at one of the shifts is equal to 1 in m_{co}, then any neighboring voxel (defined by the extent of the kernel) with a zero value would be replaced with 2 (defining the transition region) and any other voxels equal to 1 is copied in the composite mask. However, if the center voxel of the kernel mask was not set (i.e. value = 0), then a zero value is copied to the composite mask and no other action would be taken and the technique would skip and march to the next voxel in m_{co} mask.

Once the dilation process is performed, a composite mask is generated and is defined in Eq. 4 and demonstrated in Fig. 4:

$$\left.\begin{aligned} & m_{composite}(x,y,z)= \\ & \begin{cases} 2 \text{ defines the transition region} \\ 1 \text{ defines high CT number bone} \\ 0 \text{ defines every other tissue} \end{cases} \end{aligned}\right\} \quad (4)$$

The region of the mcomposite mask that contains values equal to two corresponds to the transition region of the bone diffused into the surrounding tissue. This composite mask was used with the adaptive median filter to process the bone-vessel and bone-background transition regions which will be discussed in the next section.

Filtered Transition Region Obstacle Data

$i_{af}(x, y, z)$ was generated using Eq.s 2, 3, 4 and an adaptive median filter. An adaptive median filter was applied on $i_2(x, y, z)$ data set using $m_{composite}(x, y, z)$ mask with a 3x3x3 kernel size as shown in Eq. 5:

$$\left.\begin{aligned} & i_{af}(x,y,z)= \\ & \begin{cases} median(i_2(x,y,z)) \\ \qquad \text{if } m_{composite}(x,y,z)=2 \\ i_2(x,y,z) \\ \qquad \text{if } m_{composite}(x,y,z)<2 \end{cases} \end{aligned}\right\} \quad (5)$$

Note that the adaptive median filter was only used where low CTN for bone residue exists. Voxel values which had low CTNs for bone were replaced by non bone neighboring voxel values. Although this step filters the data, note that it does not include any new values. The median filter then uses lower neighboring values to replace the remaining obstacle bone data.

Once the composite mask and the filtered data are available, the up-sampling process will need to perform and to generate the final output CTA data as shown in Fig. 1.

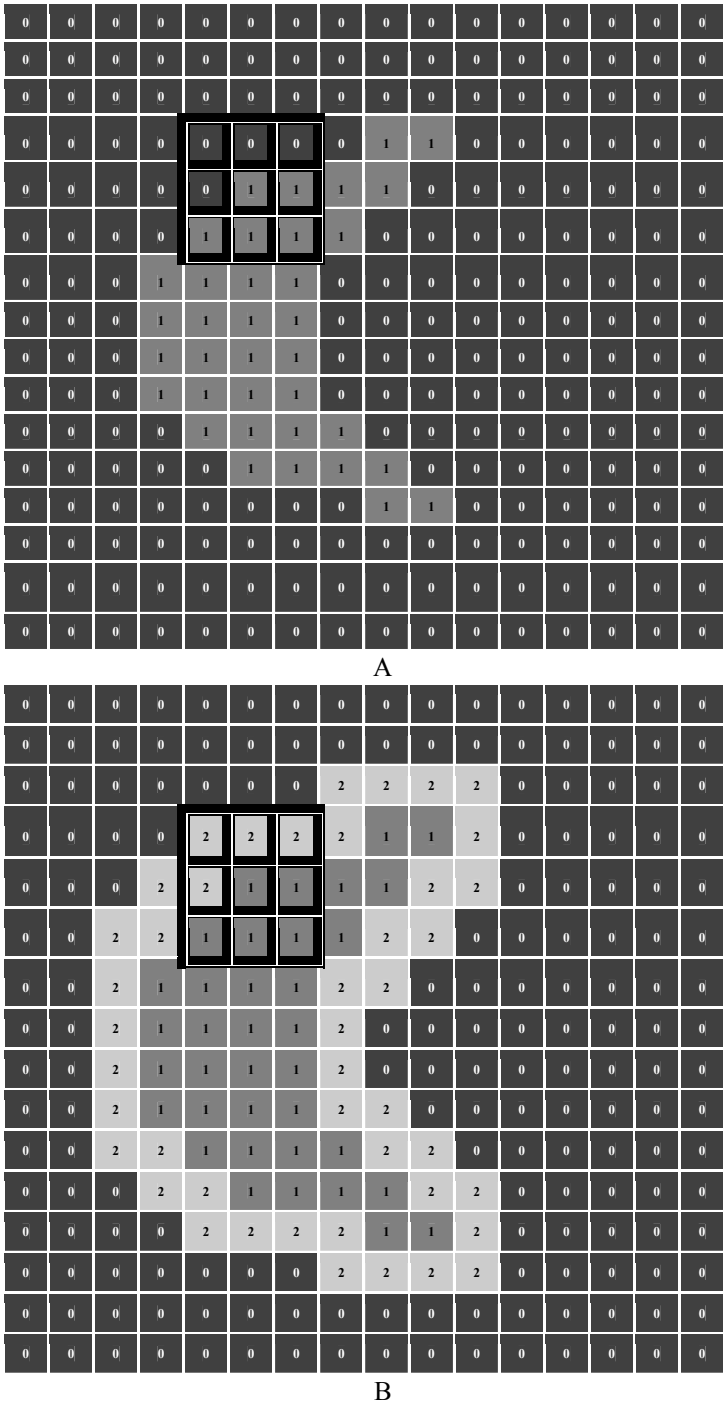

FIG. 4. Illustrates a 2-D mockup example of a dilation technique with a 3x3 kernel outlined in dark lines. Fig. 4A shows the mockup bone region. Fig. 4B shows the outcome of the dilation. Regions with values of 2, 1, and 0 correspond to the transition region, bone region, and other tissue region respectively.

Data Up-Sampling

$i_{af}(x, y, z)$ data and $m_{composite}$ masks were interpolated and up-sampled to the original spatial resolution 512x512xN (N is the original number of slices) and I_{af} and $M_{composite}$ were generated respectively. Adaptive Trilinear Interpolation using $m_{composite}$ mask was used to generate I_{af} data set as shown in Eq. 6 and voxel replication was used to produce the high resolution composite mask $M_{composite}$.

$$I_{af}(x,y,z) = \begin{cases} Trilinear\left(i_{af}(x,y,z)\right) \\ \quad \text{if } m_{composite}(x,y,z) = 2 \\ t_0 \\ \quad \text{if } m_{composite}(x,y,z) < 2 \end{cases} \quad (6)$$

The Final Output CTA with Total Obstacle Exclusion

The final step in the developed technique was to generate the final output V(x, y, z) data set using the original high resolution CTA data I(x, y, z), composite mask $M_{composite}$, the processed data $I_{af}(x, y, z)$, and t_0 as shown in Equation 7:

$$V(x,y,z)=\begin{cases} I(x,y,z) \\ \quad \text{if } M_{composite}(x,y,z)=0 \\ t_0 \ \text{ if } \ M_{composite}(x,y,z)=1 \\ I_{af}(x,y,z) \\ \quad \text{if } M_{composite}(x,y,z)=2 \end{cases} \quad (7)$$

V(x, y, z) data set contains the original vascular data, the processed data, and t_0 which replaced the high CTN for bone.

Results and Discussion

Fig. 5 illustrates the outcome of the main steps for the developed technique. Fig. 5A shows a down-sampled CTA image. The outcome of the thresholding step (threshold t_1 = 400) is illustrated by Fig. 5B showing the values below the threshold and Fig. 5C showing the values above the threshold t_1. Fig. 5D shows the connected bone region. The composite mask showing clearly the transition region as a bright line around the connected bone region is displayed in Fig. 5E. Lastly, Fig. 5F shows the outcome of implementing the proposed technique using the composite mask (Eq. 7).

The proposed technique was successful in excluding bone (obstacle data) from all ten acquired CTA data. The 3-D rendered images (MIP, SSD, VR) of the pre- and post-processed data were compared visually and assessed by an expert medical physicist. Clearly the post-processed rendered images outperformed the pre-processed rendered images. An example of this performance was demonstrated in Fig. 6. It took approximately 1 minute of CPU time on a low end workstation to segment bone, which makes the technique clinically feasible as well.

The 3-D visualization MIP technique applied on a pre- and post-processed CTA Data is shown in Fig. 6. Note that bone was totally removed and a simple MIP would provide essential diagnostic information of vessels such as the aneurysm and the calcifications as shown in Fig.s 6B and 6F. Another 3D visualization technique, such as surface shaded display, is demonstrated in Fig.s 6C and 6D. It performed similarly on the processed data in comparison to the unprocessed data.

The developed technique consists of two main ideas: the first idea explains the steps involved in the segmentation technique and the second idea consists of steps that make this technique fast and clinically feasible. The latter part involves the down-sampling and un-sampling steps of the CTA data.

Threshold and Connectivity Masks

To mark voxels that are fully filled with one specific tissue is an easy task if each tissue in an image has a separate distribution of CTNs. The difficulty arises when a voxel contains more than one tissue. This is referred to as a partial volume averaging (PVA). The spread of the CT value distribution of a tissue increases due to the PVA effect. This is most prominent between tissues with high contrast, such as the cortical bone and air filled cavities.

To select a threshold for marking a specific tissue, it should have a value below most of the tissue of interest and above the other tissues. The default t_1 threshold used in Equation 1 (400 CTN) was high enough to mark the bone (high CTNs) and to unmark air, soft tissue, and enhanced vessels in the $m_{th}(x, y, z)$ mask. Unfortunately, some vessels and calcification were also marked in m_{th} mask because of their high CTNs.

FIG. 5A

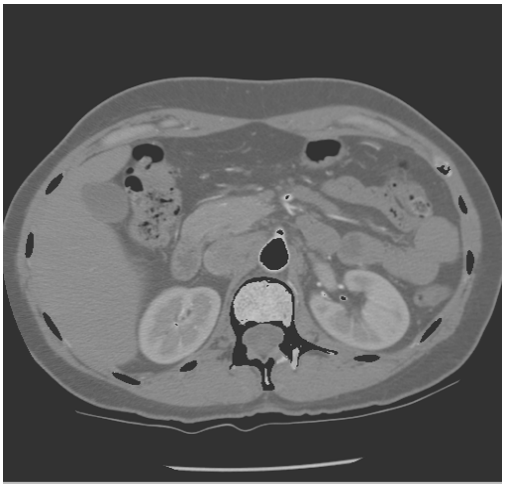

FIG. 5B

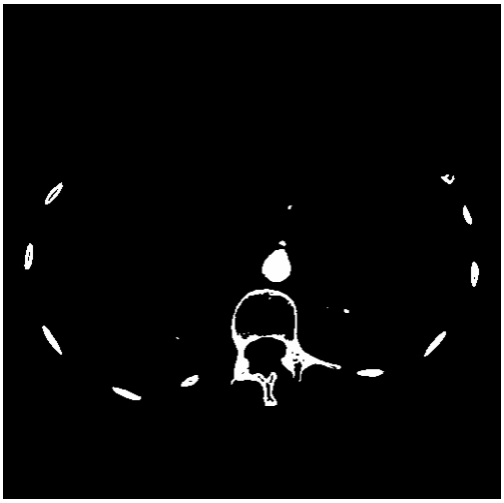

FIG. 5C

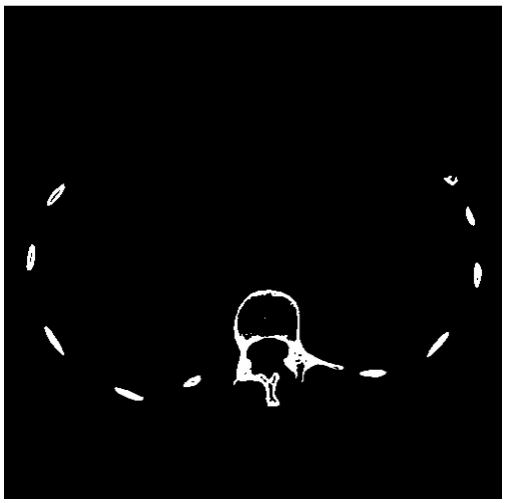

FIG. 5D

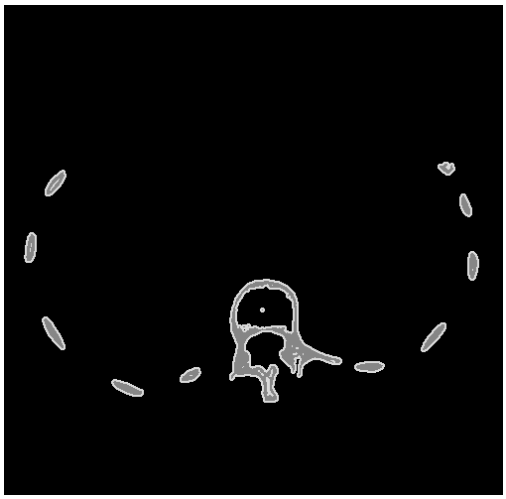

FIG. 5E

FIG. 5F

FIG. 5. Output images of different steps of the proposed technique. Fig.s 5A-5F show the original CTA image, the threshold image with CT values below bone tissues, the threshold image with CT values above bone tissues, connectivity image, the composite mask image, the processed CTA data respectively.

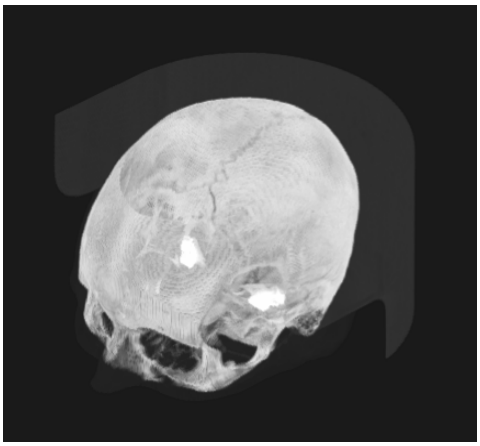

FIG. 6A

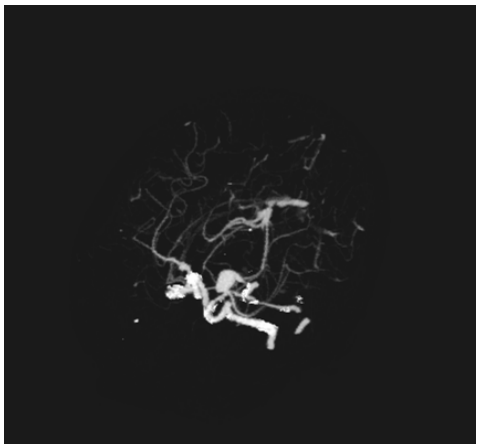

FIG. 6B

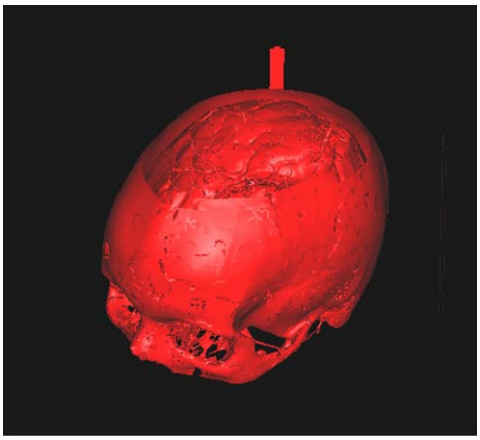

FIG. 6C

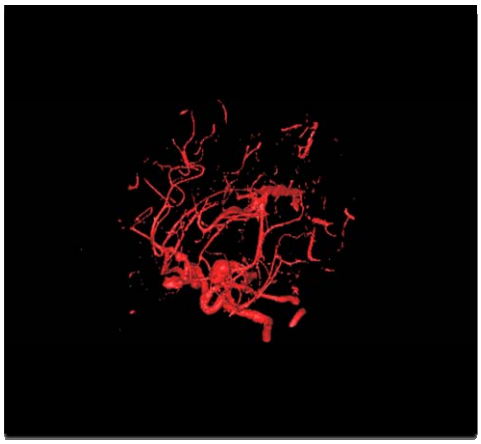

FIG. 6D

FIG. 6E

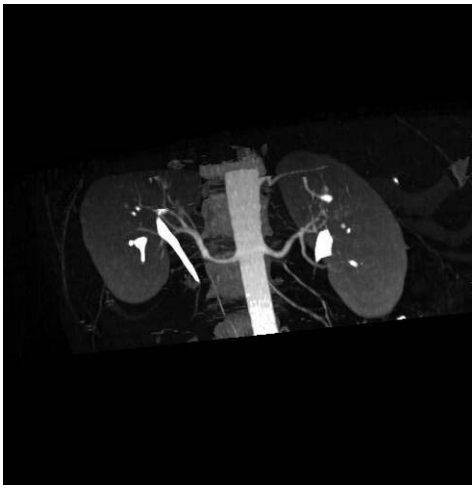

FIG. 6F

FIG. 6. Illustrates maximum intensity projection images and surface shaded display images of CTA data. Fig.s 6A and 6B show MIP images of unprocessed and processed head CTA data respectively. Fig.s 6C and 6D show surface shaded display images of unprocessed and processed head CTA data respectively. Fig.s 6E and 6F show MIP of unprocessed and processed abdomen CTA data respectively.

Note that t_1 threshold can be adjusted by the user for optimal processing. Increasing t_1 beyond the proposed limit (350 – 500 CTN) would provide a higher probability of not masking vessels or calcifications. This would increase the transition region and thus the filtered data and the processing time. Decreasing t_1 beyond the proposed limit reduces the transition region and thus the filtered data and processing time. This leads to a higher probability in removing vessels and calcifications.

Calcifications however, were generally located internal to the vessels and were not connected to bone. Therefore, the connectivity m_{co} mask was used to unmark voxels from the m_{th} mask corresponding to high CTNs for calcifications in $i(x, y, x)$ and to retain marked voxels corresponding to bone. Note that connected bone (i.e., fragment bone) would not be in the m_{co} mask if a single seed was used. Fragmented bone was removed however by selecting multiple seeds, some of which were within the fragmented bone. Selecting multiple seeds was easily accomplished by using a high threshold (i.e. default threshold was equal to 90% of the maximum in the data) applied on $i(x, y, z)$ data. Voxels containing CTNs higher than this high threshold were all bone. Voxels containing calcification were still below this threshold.

Note that the s_1 threshold can also be adjusted by the user for optimal processing. Increasing s_1 beyond the proposed limit (90% of maximum CTN) would provide higher accuracy of selecting seeds for the connectivity technique. This however would lead to the decrease in the number of seeds which may lead to non-removal of some fragmented bone. Decreasing s_1 beyond the proposed limit reduces increases the number of seeds for the connectivity algorithm. This leads to a higher probability in marking seeds in the lower CTN region thus removing vessels and calcifications.

For optimal results in excluding bone using the proposed technique, the threshold t_1 in the all CTA data sets ranged from 350- to 500 CTN. This variation was related to the PVG effect and to the variation in the CTNs for enhanced vessels. This variation is related to the variation of the amount of contrast agents contained within the vessels. In addition, this can be attributed to inter-subject bloodstream variability.

Note that thresholding and connectivity still do not guarantee that all bone is marked. Voxels with (low CTNs for bone) contained partially bone and partially other tissues which were not marked in either the m_{th} or the m_{co} mask.

Exclusion of High CTN Obstacle Data

This step retains the $i(x, y, z)$ CTA data in $i_2(x, y, z)$ except for high CTNs of bone. High CTNs for bone were excluded based on the m_{co} mask. Nevertheless, $i_2(x, y, z)$ still contains partial bone that has CT values lower that t_1 (Eq. 1). Note that the thresholding step generated sharp edges between t_0 region (where high CTN bone used to be) and low CTN bone. These false edges are removed by applying an adaptive smoothing filter as described later in this section.

Transition Region and Composite Mask

Some voxels containing partial bone still have higher CTNs than enhanced vessels, and would still provide obstacles in 3D visualization. The dilation step expands the bone region in the m_{co} mask such that it covers voxels with partial bone in $i(x, y, z)$ (Eq.s 3 and 4).

Without the down-sampling step, the dilation kernel needs to be larger (i.e. 5x5x5 or even 7x7x7) to mark the transition region in the original data. Because voxels containing partial bone in the high resolution original data fall off more gradually and cover larger voxel area. Although, a larger kernel even guarantees more mapping of partial bone, the heavy price to pay is the processing time which renders a technique with the current technology clinically challenging. Even though the resolution is reduced with down-sampling, but the benefits are two-fold. First, the amount of data is reduced which means less data to process, and second, the dilation kernel is smaller, a 3x3x3 kernel size is sufficient to mark the transition region. The drawback of down-sampling is that it may cause loss of some details or resolution in the transition region.

Filtered Transition Region Obstacle Data

An image processing filter (i.e. mean, Gaussian, or any other smoothing filter) can be used in this step to replace the low CTNs for bone voxels. However, a median filter provides a more accurate representation or replacement. It removes speckles while preserving true edges in the data [19,20].

For voxels containing multiple tissues, a dominant structure (i.e. bone) tends to overshadow the other tissues. The role of the adaptive median filter here is to use the median dominant structure (i.e. soft tissues) instead of the dominant structure in the replacement process. The existence of partial bone in a voxel would give that voxel a high CTN, although there might be more volume from other tissue in that voxel bone. With the use of a median filter, the low CTN for bone is replaced with neighboring voxels which may be vessels, soft tissue, or air. A median filter would cause other tissues to grow into the bone transition region instead of having the bone grow into the other tissue.

If this process was performed on the original data I(x, y, z) then a larger kernel size would be needed to filter out the low CTNs for bone. Therefore down-sampling is necessary to make this technique feasible for clinical use.

Down-Sampling, Up-Sampling and Composite Data

Down-sampling is done using the maximum CTN of the kernel instead of the minimum, the mean or any other voxel value within the kernel. If the minimum is used in the down-sampling process, some high CTNs for bone are removed by that process alone, but the surrounding voxels would still contain low CTNs for bone. The transition region next to the high CTN for bone voxels cannot be generated which leads to the inability of removing the low CNTs for bone. More importantly with a minimum value down-sampling process, if vessels and air are in the down-sampling kernel, vessels will be replaced with air which would cause a loss of some vessel information as well.

In addition, if the mean value is used in the down-sampling process, it would smooth the data and would contribute to changing the values of the vessels and other structures in the CTA data. Using the maximum CTNs in the down-sampling process guarantees that the high CTNs for bone will be in the low resolution data and the transition region can be generated to remove the low CTNs for bone. In addition, there will be no change to vessel information for reasons discussed in the previous paragraph.

Since the original CTA data was not isotropic, another advantage to the down-sampling step in the manner described in this paper is the generation of the down-sampled isotropic data. This makes the kernels, used in filtering the data, have equal weighting for filtering which leads to proper and easier processing.

Current CT scanners can produce many more slices than processed in this paper. This leads to more CT slices to diagnose and process which increase the demand to make the technique faster. This emphasizes the use of the down-sampling idea presented in this paper. Displaying cine' 2-D images or volume render a small volume of interest (VOI) with a linear transfer functions are currently clinically used to display the CTA data [21, 22, 23]. Clearly this requires time as well as experience in adjusting and understanding the transfer function used [24]. Fig. 7 shows a MIP rendered image of a small VOI of the original data (unprocessed data) which took approximately 10 minutes of preparation.

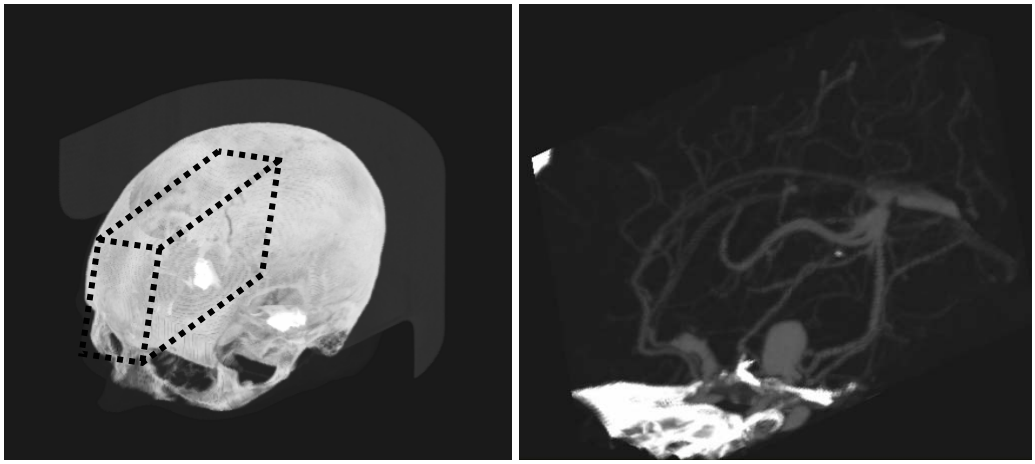

A B

FIG. 7. illustrates MIP volume rendered images of the original CTA data. Fig. 7A is a MIP image of the whole original data; and Fig. 7B is a MIP image of a volume of interest roughly shown as a dotted box on Fig. 7A

Trilinear interpolation is a costly process in terms of time. Nevertheless it was needed to interpolate the processed data $i_{af}(x, y, z)$ because of its superior output image quality. Voxel replication is a faster process than trilinear interpolation but it provides poorer output image quality. Voxel replication was used with the generated masks because interpolating binary data using a trilinear technique does not improve the output image quality unless the data is changed to have more than binary values. Voxel replication of the composite mask was a sufficient technique to provide overall acceptable image quality.

The interpolation step prepares all the needed data sets for the composition of the final output data. This data set contains all the diagnostic information of vessels and calcification without the bone barrier. A 3-D Visualization technique can then be used to easily display the vascular content of this data. Note that the developed technique proposed here is to aid radiologists in the vessel visualization and diagnosis but by no means is intended to replace the original CTA data set.

The developed technique may encounter few limitations. This technique may be sensitive to the amount of contrast agent injected into the patient. Increasing the contrast agent may lead to increase the vessels CTNs to the level of bone. This may lead to the removal of the bone and some of the vessels data. In addition, the technique may remove high CTN calcifications in vessels touching the bone region. However, this can be resolved by editing and removing any seed that falls in the calcifications region. Furthermore, the developed technique requires large amount of memory to process multiple inputs simultaneously. This demand on memory is emphasized with large size data set. However, the down-sampling process of the data should reduce the amount of memory for processing.

Finally, we hypothesize that our technique can be used on CTA data for other regions of the body. This is currently under investigation.

Summary

In this paper we have described a technique that is useful in excluding barrier structure (i.e. bone) from CTA data to unveil important diagnostic vessel information. The novel aspects of this technique are its ability to retain the vasculature data in pristine form and the removal of bone leaving out very little residue. We have also described ways to expedite processing with very little compromise to the image accuracy. We have demonstrated the usefulness of the technique and its visual accuracy on clinical data examples for the Circle of Willis region as well as the abdominal region. We argue that our bone removal technique would improve the diagnostic quality of 3-D visualization techniques such as MIP, SSD, and VR. These 3-D visualization techniques of the output data clearly show by visual inspection the 3-D vessel information.

References

[1]Schwartz, R.B., Jones, K.M., Cernoff, D.M., Mukherji, S.K., Khorasani, R., Tice, H.M., Kikinis, R., Hooton, S.M., Steig, P.E. and Polak, J.F., Radiology, 185 (1992) 2.

[2]Caplan, L.R. and Pessin, M.S., Annual Rev. Med. 39 (1988) 273.

[3]Marks, M.P, Napel, S., Jordan, J.E. and Enzmann, D.R., American J. of Radiology, 160 (1993) 1267.

[4]Kuszyk, B.S., Heath, D.G., Bliss, D.F. and Fishman, E.K., Skeletal Radiology, 25 (1996) 207.

[5]Webber, G., Dillard, S., Carr, H., Pascucci, V. and Hamnn, B., IEEE Transactions on Visualization and Computer Graphics, 13(2) (2007) 330.

[6]Lorensen, W.E. and Cline, H.E., Marching Cubes, Computer Graphics (Proceedings of SIGGRAPH), 21(4) (1987) 163.

[7]Alyassin, AM, Lancaster, J.L., Downs III, J.H. and Fox, P.T., Medical Phys. 21(6) (1994).

[8]Lancaster, J.L., Eberly, D., Alyassin, AM, Downs III, J.H. and Fox, P.T., Medical Phys. 19 (1992) 419.

[9]Dake, M.D., McDonnnel, C.H, Song, S.M., Enzmann, D.R., Napel, S., Marks, M.P., Rubin, G.D. and Jeffrey, R.B., Radiology, 185 (1992) 607.

[10]Napel, S.A., "Principles and techniques of 3D spiral CT angiography, "In Spiral CT: Principles, Techniques and Clinical Applications" Eds. E.K. Fishman and R.B. Jeffery Jr., (Raven Press Ltd., New York, 1995), p.169.

[11]Cline, H.E., Lorensen, W.E., Kikinis, R. and Jolesz, F., J. of Computer Assisted Tomography, 14(6) (1990) 1037.

[12]Shiffman, S., Rubin, G. and Napel, S., SPIE, 2707 (1996) 140.

[13]Bani-Hashemi, A., Krishnan, A. and Samaddar, S., SPIE, 2710 (1996) 428.

[14]Van Tran, L. and Sklansky, J., IEEE Trans. Medical Imag. 11(3) (1992) 407.

[15]Urshler, M., Ditt, H. and Bischof, H., "Partially Rigid Bone Registration in CT Angiography" Eds. Computer Vision Workshop, Ondrej Chum Vojtech Franc, (2006), p.1.

[16]Alyassin, A.M. and Avinash, G.B., In Sonka, M. and Hanson, K.M., editors, Proceedings of SPIE: Medical Imaging: Image Processing, 4322 (2001) 1273.

[17]Braga-Neto, U. and Goutsias, J., J. of Mathematical Imaging and Vision, 19 (2003) 5.

[18]Ronse, C., Najman, L. and Decencière, E., Math. Morphology: 40 Years On, (Eds.), ISBN-10 (2005) 1-4020-3442-3.

[19]Jiang, J. and Crookes, D., Electronics Letters, 42(24) (2006) 1379.

[20]Toprak, A. and Güler, İ., J. of Medical Systems, 30(6) (2006) 465.

[21]Rubin, G.D. and Rofsky, N.M, "CT and MR Angiography: Comprehensive Vascular Assessment", (Lippincott Williams & Wilkins, Philadelphia, 2008).

[22]Verhoek, G., Philip, K., Ee, W., Wu, R., Kat, E. and Fitridge, R.A., J. of Computer Assisted Tomography, 23(4) (1999) 590.

[23]McKinneya, A.M., Palmera, C.S., Truwita, C.L., Karagullea, A. and Teksamb, M., American J. of Neuroradiology, 29 (2008) 594.

[24] Alyassin, AM, Proceedings of SPIE Medical Imaging – Visualization, Image Guided Procedures, and Display, 4681 (2002) 338.